

THE PERSISTENCE OF MEMORY, OR HOW THE X-RAY SPECTRUM OF SNR 0509–67.5 REVEALS THE BRIGHTNESS OF ITS PARENT TYPE IA SUPERNOVA

CARLES BADENES^{1,2,3}, JOHN P. HUGHES^{1,2}, GAMIL CASSAM-CHENAI¹, AND EDUARDO BRAVO⁴

Draft Version July 27, 2021

ABSTRACT

We examine the dynamics and X-ray spectrum of the young Type Ia supernova remnant 0509–67.5 in the context of the recent results obtained from the optical spectroscopy of its light echo. Our goal is to estimate the kinetic energy of the supernova explosion using *Chandra* and *XMM-Newton* observations of the supernova remnant, thus placing the birth event of 0509–67.5 in the sequence of dim to bright Type Ia supernovae. We base our analysis on a standard grid of one-dimensional delayed detonation explosion models, together with hydrodynamic and X-ray spectral calculations of the supernova remnant evolution. From the remnant dynamics and the properties of the O, Si, S, and Fe emission in its X-ray spectrum we conclude that 0509–67.5 was originated ~ 400 years ago by a bright, highly energetic Type Ia explosion similar to SN 1991T. Our best model has a kinetic energy of 1.4×10^{51} erg and synthesizes $0.97 M_{\odot}$ of ^{56}Ni . These results are in excellent agreement with the age estimate and spectroscopy from the light echo. We have thus established the first connection between a Type Ia supernova and its supernova remnant based on a detailed quantitative analysis of both objects.

Subject headings: ISM: individual (SNR 0509–67.5) — nuclear reactions, nucleosynthesis, abundances — supernovae: general — hydrodynamics — supernova remnants — X-rays:ISM

1. INTRODUCTION

Astronomical observations can probe the material ejected by supernova (SN) explosions during two transient phases with very different time scales. The initial optical transient (the SN itself) lasts for several months, and the ejecta structure can be studied through the emission and absorption lines produced as the photosphere recedes into the exploded star. After the SN fades away, the ejected material starts to interact with its surroundings, and the supernova remnant (SNR) phase begins. In this phase, the ejecta structure is revealed by the X-ray emission of the material heated by the reverse shock on timescales of hundreds or thousands of years. Both approaches are valid in principle, but up to now the disparity of the timescales involved has made it impossible to verify their mutual consistency by applying them to the same object.

The serendipitous discovery of light echoes associated with the young SNRs 0509–67.5, 0519–69.0, and N103B in the Large Magellanic Cloud (LMC) by Rest et al. (2005) (henceforth R05) has opened new possibilities for establishing connections between SNRs and their parent SNe. In particular, spectroscopy of the light echoes has the potential to confirm the type of the SN explosion in a straightforward way, avoiding the difficulties inherent to typing SNRs from their X-ray spectra (for an in-

depth discussion of these difficulties, see Rakowski et al. 2006). In a recent paper, Rest et al. (2007) (henceforth R07) examined the light echo associated with SNR 0509–67.5, and established that this object originated in a Type Ia explosion, in agreement with the longstanding claims based on X-ray observations (Hughes et al. 1995; Warren & Hughes 2004, henceforth WH04). Furthermore, the quality of the light echo was such that it allowed for a meaningful comparison with the spectra of a variety of Type Ia SNe. Based on these comparisons, R07 concluded that the parent event of SNR 0509–67.5 belonged to the group of overluminous, highly energetic Type Ia SNe whose prototype is SN 1991T (Benetti et al. 2005).

These results offer an excellent opportunity to revisit the X-ray spectrum of SNR 0509–67.5. Recent developments in modeling the thermal emission in young Type Ia SNRs using hydrodynamic calculations and nonequilibrium ionization simulations (HD+NEI models, Badenes et al. 2003, 2005a) have led to a better understanding of the relationship between the structure of SN ejecta and the X-ray spectra of SNRs. By applying HD+NEI models to the Tycho SNR, Badenes et al. (2006) were able to estimate the kinetic energy and nucleosynthetic yields of the explosion. We can now do the same for 0509–67.5, comparing the results of the HD+NEI models with the light echo spectroscopy. In particular, we want to examine to what extent is it possible to determine the brightness of a Type Ia SN by studying the X-ray emission from its SNR hundreds of years after the explosion.

This paper is organized as follows. In § 2, we begin with a brief overview of delayed detonation models. In § 3, we use these explosion models, together with the forward shock radius and velocity to constrain the dynamics of SNR 0509–67.5. In § 4, we review the *Chandra*

¹ Department of Astrophysical Sciences, Princeton University, Peyton Hall, Ivy lane, Princeton, NJ 08544-1001; badenes@astro.princeton.edu

² Department of Physics and Astronomy, Rutgers University, 136 Frelinghuysen Rd., Piscataway NJ 08854-8019; jph@physics.rutgers.edu, chenai@physics.rutgers.edu

³ *Chandra* Fellow

⁴ Departament de Física i Enginyeria Nuclear, Universitat Politècnica de Catalunya, Diagonal 647, Barcelona 08028, Spain; and Institut d'Estudis Espacials de Catalunya, Campus UAB, Facultat de Ciències. Torre C5. Bellaterra, Barcelona 08193, Spain; eduardo.bravo@upc.es

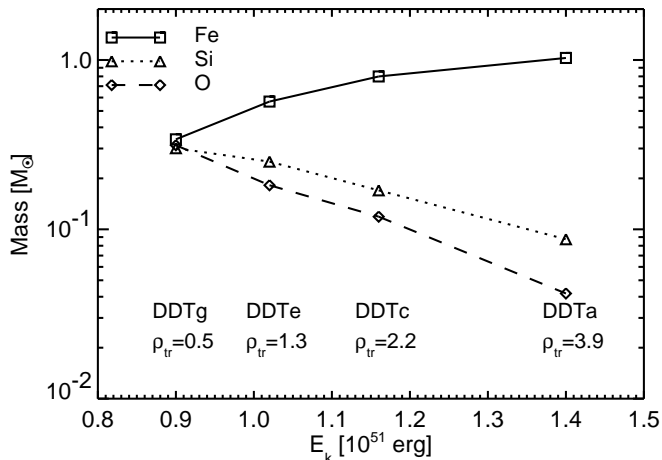


FIG. 1.— Nucleosynthetic yields of Fe (after radioactive decays, solid line, squares), Si (dotted line, triangles), and O (dashed line, diamonds) in the DDT models as a function of E_k . Each model is labeled in the plot, indicating the corresponding value of ρ_{tr} in units of 10^7 g cm^{-3} .

and *XMM-Newton* observations of 0509–67.5, and we calculate the values for the most relevant line centroids and line flux ratios. In § 5 we describe the HD+NEI models, and we evaluate them against both the dynamic and spectral constraints posed by the observations of 0509–67.5. Finally, we discuss our results and present our conclusions in § 6.

2. OVERVIEW OF DELAYED DETONATION MODELS

Since they were first introduced by Khokhlov (1991), delayed detonations (DDTs) have become the most successful models for Type Ia SNe. In this kind of explosion, the burning front starts propagating as a subsonic flame (deflagration) in the central regions of a C+O white dwarf (WD) close to the Chandrasekhar mass, and then a transition to a supersonic regime (detonation) is artificially induced, usually at a prescribed density ρ_{tr} . The resulting ejecta structure is characterized by an approximately exponential density profile, with a composition dominated by Fe-peak nuclei in the center, surrounded by a shell rich in intermediate mass elements (IMEs: Si, S, Ar, Ca, etc.), and a thinner outer region dominated by O. Minor traces of C might remain at large radii, but most of the WD is burnt in the explosion. Spherically symmetric DDT models are able to explain the fundamental properties of Type Ia SNe, including light curve shapes (Höflich & Khokhlov 1996), optical and IR spectral evolution (Wheeler et al. 1998; Baron et al. 2006; Marion et al. 2006; Gerardy et al. 2007), and spectropolarimetric observations (Wang et al. 2007).

The deflagration-to-detonation transition density ρ_{tr} is the most important parameter in DDT explosions. Models with higher values of ρ_{tr} are more energetic, and synthesize more Fe-peak elements, less IMEs, and less O than models with low values of ρ_{tr} . Since Type Ia light curves are powered by the radioactive decay of ^{56}Ni , more energetic models lead to more luminous SNe (Stritzinger et al. 2006). The luminosity of Type Ia SNe is also tightly correlated to the light curve width (Phillips 1993), although the physical processes connecting this parameter and the mass of ^{56}Ni synthesized in the explosion are not as simple as was initially thought (see Kasen & Woosley 2007; Woosley et al. 2007). In any

case, the relationship between Type Ia SN luminosity (or light curve width) and the chemical structure of SN ejecta has now been firmly established by Mazzali et al. (2007), and is consistent with the predictions of one-dimensional DDT models.

The fundamental properties of the grid of DDT models that we will use in the present work are plotted in Figure 1, which can be compared to the ‘Zorro’ diagram in Mazzali et al. (2007). Models DDTa, DDTc, and DDTe are taken from Badenes et al. (2003, 2005a); model DDTg has been calculated with the same code (see Bravo et al. 1996; Badenes et al. 2003), and extends the grid to lower values of E_k . The total masses of ^{56}Ni synthesized in the models are $0.97 M_{\odot}$ (DDTa), $0.74 M_{\odot}$ (DDTc), $0.51 M_{\odot}$ (DDTe), $0.29 M_{\odot}$ (DDTg). To put these values in context, the estimated ^{56}Ni masses in the 20 objects considered ‘normal’ by Mazzali et al. (2007) range between $0.94 \pm 0.05 M_{\odot}$ (for SN 1991T) and $0.24 \pm 0.05 M_{\odot}$ (for SN 1991M). A theoretical upper limit to the mass of radioactive Ni that can be obtained from the thermonuclear burning of a Chandrasekhar C+O WD is set by the prompt detonation model DET in Badenes et al. (2003), which yields $1.16 M_{\odot}$ of ^{56}Ni with $E_k = 1.6 \times 10^{51}$ erg.

3. SNR DYNAMICS

The dynamics of 0509–67.5 are constrained by two pieces of observational evidence. The first is the angular radius measured by *Chandra* (15.1”, see Table 3 in Badenes et al. 2007), which translates into a linear radius of 1.1×10^{19} cm (3.7 pc) at the known distance to the LMC (50 kpc, Alves 2004). This measurement can be considered very accurate, because the errors on both angular radius and distance are extremely small (at the few percent level). The second observable is the forward shock (FS) velocity inferred by modeling the broad component of the $\text{Ly}\beta$ emission line, $3600 - 7100 \text{ km s}^{-1}$ (Ghavamian et al. 2007). Being a less direct measurement, the FS velocity is more subject to uncertainty than the FS radius, so this value should be considered with some measure of caution (see discussion in § 5.1 of Badenes et al. 2007). To reproduce the dynamics of 0509–67.5, we have used a one-dimensional hydrodynamic code to simulate the interaction between the ejecta density profiles from the DDT explosion models in our grid and a uniform ambient medium (AM; for more details on the models and a justification of the uniform AM hypothesis, see Badenes et al. 2007). A successful SNR model must be able to match both FS radius and velocity for a reasonable combination of age t and AM density ρ_{AM} .

The comparison between hydrodynamic models and observations, however, is not completely straightforward, because our simulations do not include the effect of cosmic ray (CR) acceleration. This physical process can strongly modify the dynamics of the SNR, slowing down the FS and reducing the gap between FS and contact discontinuity (CD) by an amount that depends on the acceleration efficiency (Ellison et al. 2004). Indeed, WH04 found evidence for a significant nonthermal component in the X-ray spectrum of 0509–67.5 and argued that CR acceleration was taking place at the FS. Although the presence of nonthermal emission does not necessarily im-

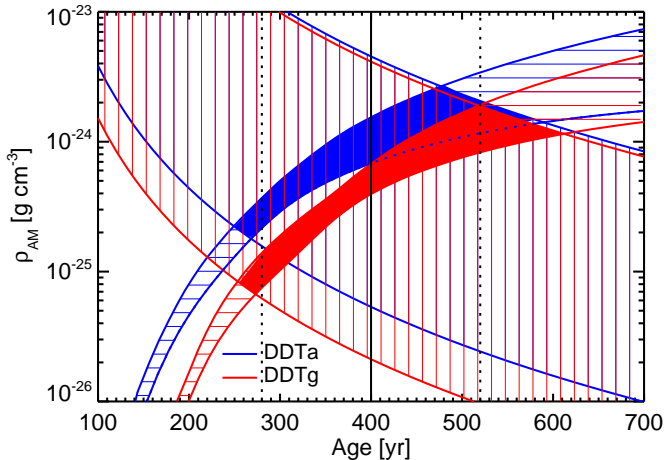


FIG. 2.— Constraints on the dynamics of 0509–67.5 from the observed FS radius and velocity. The horizontally striped areas indicate the regions of the parameter space where the FS radius lies between R_{FS} and $1.1 \times R_{CD}$ in models DDTa (blue) and DDTg (red). The vertically striped areas indicate the regions of the parameter space where the FS velocity lies between u_{FS} and u_{CD} in each model. The areas where both constraints overlap are highlighted with solid colors. The age estimate from the light echoes is represented with the vertical solid and dotted lines.

ply that the dynamics are CR-modified, we consider this to be a likely possibility. It is important to note that CR acceleration at the FS does not have an impact on the dynamics of the shocked ejecta, and in particular, it does not affect the position of the CD (at least to first order, see Fig. 2 in Ellison et al. 2007). This means that the CR-modified SNR radius must lie between the FS radius R_{FS} and the CD radius R_{CD} in hydrodynamic models without CR acceleration. For one-dimensional models, it is necessary to allow for the fact that Rayleigh-Taylor instabilities at the CD increase the projected radius by $\sim 10\%$ (Wang & Chevalier 2001). Likewise, the CR-modified FS velocity must lie between the FS velocity u_{FS} and the CD velocity u_{CD} . We have summarized these constraints in Figure 2 for the most and least energetic models in our DDT grid, DDTa and DDTg. The DDT models require that the SNR age be between 250 and 610 yr to reproduce the FS dynamics, in very good agreement with the completely independent 400 ± 120 yr estimate from the light echoes (R05). The allowed values of ρ_{AM} lie between 5×10^{-26} and 2×10^{-24} g cm^{-3} , with more energetic models demanding higher AM densities. The FS radius provides the strongest dynamical constraints, imposing a tight correlation between ρ_{AM} and age that we shall revisit in § 5.3.

4. X-RAY OBSERVATIONS

4.1. *Chandra* and *XMM-Newton* Data Sets

SNR 0509–67.5 has been observed by the CCD cameras on both *Chandra* and *XMM-Newton*. The most detailed study of its X-ray emission to date was presented by WH04, who analyzed a *Chandra* ACIS-S data set taken on 2000 May 12–13 (ObsID 776, PI J.Hughes). The net exposure time was 47.9 ks, and the image was taken on the back-illuminated S3 chip. The authors found that the X-ray spectrum is dominated by line emission from the SN ejecta, with a small continuum contribution, probably nonthermal emission from the FS. The centroid of the Si $K\alpha$ line blend indicates an unusually low (below

He-like) ionization state for the plasma. The abundances obtained from plane-parallel shock fits favor a Type Ia origin, in agreement with the previous qualitative analysis of Hughes et al. (1995). These abundances were compared to the yields of two type Ia SN explosion models from Iwamoto et al. (1999), a ‘fast deflagration’ and a DDT, with the fitted values showing some preference for the DDT model, albeit with gross discrepancies in the Fe abundance that were noted by the authors. This might be due to the simplicity of the plane shock models used by WH04, but the poor statistics of the Fe $K\alpha$ blend in the *Chandra* ACIS-S data set also make it difficult to constrain the properties of shocked Fe in 0509–67.5.

For the present work, we have recalibrated the *Chandra* ACIS-S data using the latest versions of CIAO (3.4) and CALDB (3.4.0), which yielded 48.5 ks of useful exposure. To complement the *Chandra* data set, we have also reduced and analyzed the *XMM-Newton* observation taken on 2000 July 4 (ObsID 0111130201, PI M.Watson). The instrument modes in this observation were small window for EPIC-MOS1 (frame time: 300 ms), large window for EPIC-MOS2 (900 ms) and EPIC-pn (48 ms). The medium filter was used. We reduced the data using the latest SAS version (7.1.0) and calibration files. We applied the flare rejection procedure described in Cassam-Chenai et al. (2004), which left a total exposure of 32.6 ks for all cameras. To create spectra, we selected single and double events (pattern ≤ 4) for the EPIC-pn camera, which greatly improved the statistics in the Fe $K\alpha$ line. The spectra were then rebinned to achieve a signal-to-noise ratio $> 3\sigma$.

A preliminary inspection of the calibrated and reduced spectra reveals that the centroids of the brightest lines in the EPIC-MOS cameras appear shifted towards high energies compared to both EPIC-pn and *Chandra* ACIS-S. The Si $K\alpha$ centroid values obtained with the different CCD instruments, with standard 90% confidence intervals, are 1.850 ± 0.002 keV (EPIC-MOS1), $1.847^{+0.003}_{-0.002}$ keV (EPIC-MOS2), 1.834 ± 0.002 keV (EPIC-pn), and $1.833^{+0.003}_{-0.002}$ keV (ACIS-S). The overlap between the ACIS-S and EPIC-pn values is important, because the energy scale of the *Chandra* ACIS-S data set was verified using on-board calibration sources (see § 2 in WH04). Furthermore, EPIC-pn has a substantially larger effective area at the Fe $K\alpha$ line than EPIC-MOS. In view of this, we have chosen to maximize the consistency of our data sets by not including the EPIC-MOS spectra in our analysis. The spatially integrated *Chandra* ACIS-S and *XMM-Newton* EPIC-pn spectra are plotted in Fig. 3.

4.2. Spectral Fits to the Line Emission

We have fitted the *Chandra* ACIS-S and *XMM-Newton* EPIC-pn data between 1.6 and 8.0 keV with a spectral model consisting of a power law continuum and 16 Gaussian lines, including K-shell transitions from principal quantum level $n = 2$ ($K\alpha$ blends) for Si, S, Ar, Ca, and Fe; K-shell transitions from $n = 3, 4, 5$ ($K\beta$, $K\gamma$, and $K\delta$) for Si, S, and Ar, and the $Ly\alpha$ lines for the H-like ions of Si and S. Only the centroids and fluxes of the $K\alpha$ blends and the Si $K\beta$ line have been fitted. The centroids of the other $K\beta$ lines and all the $K\gamma$, $K\delta$, and $Ly\alpha$ lines have been kept fixed at the nominal energies for He-like ions. The fluxes of the $K\gamma$ and $K\delta$ lines have been tied to the

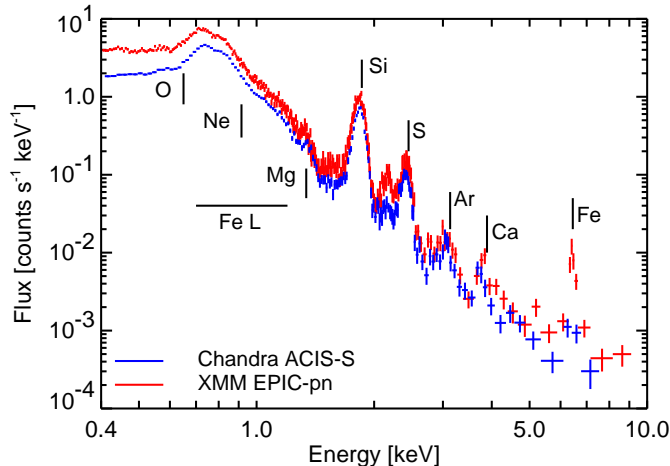


FIG. 3.— Spatially integrated spectrum from *Chandra* ACIS-S (blue) and *XMM-Newton* EPIC-pn (red). The expected centroids of the K α blend from the He-like ions of O, Ne, Mg, Si, S, Ar, and Ca are indicated for reference, as is the Fe K α blend and the region dominated by Fe L-shell lines.

respective K β lines taking the ratios at $T_e = 5 \times 10^7$ K from the ATOMDB data base (Smith et al. 2001). The resulting fits are shown on Figure 4 and the fitted parameters are listed in Table 1.

Outside the energy range of the fits, we have calculated a conservative upper limit to the O K α flux by assuming that all the photons between 0.55 and 0.58 keV come from this blend, with interstellar absorption set at the maximum value found by WH04, $N_H = 0.076 \times 10^{22}$ cm $^{-2}$. We note that the presence of O was necessary in the plane shock fits performed by WH04, and that O lines are clearly seen in the grating observations (Hughes et al. in preparation), but for this element it is especially hard to disentangle the ejecta contribution from the shocked AM contribution (if any). Thus, we settle for the conservative upper limits listed in Table 1 to constrain our ejecta models. We have also calculated the flux in the broad band from 0.8 keV to 1.2 keV, which is dominated by L-shell lines from Fe, with some contribution from K-shell Ne lines, assuming a nominal value of $N_H = 0.07 \times 10^{22}$ cm $^{-2}$. The principal line flux ratios normalized with respect to Si K α are listed in Table 2.

The values listed in Tables 1 and 2 merit a few comments. All the line centroids and line flux ratios, as well as the power law indices and normalizations, are consistent in both data sets within the statistical uncertainties. However, some puzzling differences between the *Chandra* ACIS-S and the *XMM-Newton* EPIC-pn spectra can be appreciated both in the Tables and in Figures 3 and 4. The fluxes of the three brightest lines are statistically inconsistent, with deviations of 11% for Si K α , 24% for S K α , and a very significant 34% for Si K β . The upper limits for the O K α emission and the fluxes in the broad Fe L band also show disagreements of 9% and 18%. Some of these differences are larger than the cross-calibration uncertainty between *Chandra* and *XMM-Newton*, which is 15% in normalisation between 0.8 and 2 keV (M. Stuhlinger et al., document XMM-SOC-CAL-TN-0052, Issue 3.0, January 2006). The discrepancies certainly deserve some further investigation, but they are of no consequence for the scientific objectives of this paper, for two reasons that will become clear

TABLE 1
SPECTRAL PARAMETERS IN THE SNR 0509–67.5

Parameter	<i>Chandra</i> ACIS-S	<i>XMM-Newton</i> EPIC-pn
Power Law Continuum		
α	$3.37^{+0.23}_{-0.21}$	$3.42^{+0.20}_{-0.19}$
Norm. (10^{-6} photons cm $^{-2}$ s $^{-1}$)	416^{+89}_{-74}	348^{+67}_{-57}
Line Fluxes (10^{-6} phot cm $^{-2}$ s $^{-1}$)		
O K α ^a	< 396	< 362
Fe L ^b	1177	958
Si K α	123 ± 4	110 ± 3
Si K β	11.5 ± 1.8	7.64 ± 0.89
S K α	33.3 ± 2.8	$25.4^{+1.9}_{-2.0}$
Ar K α	2.94 ± 1.02	3.56 ± 0.88
Ca K α	$0.992^{+0.71}$	1.08 ± 0.46
Fe K α	$4.60^{+2.00}_{-1.94}$	$3.32^{+0.66}_{-0.65}$
Line Centroids (keV)		
Si K α	$1.833^{+0.003}_{-0.002}$	1.834 ± 0.002
Si K β	$2.146^{+0.019}_{-0.014}$	2.161 ± 0.014
S K α	$2.415^{+0.006}_{-0.007}$	$2.422^{+0.006}_{-0.005}$
Ar K α	$3.064^{+0.027}_{-0.024}$	3.036 ± 0.042
Ca K α	$3.737^{+0.072}_{-0.060}$	$3.811^{+0.032}_{-0.033}$
Fe K α	$6.572^{+0.030}_{-0.029}$	$6.440^{+0.030}_{-0.029}$
Goodness-of-Fit		
χ^2/dof	45.1/64	135.0/130

NOTE. — The limits given are the formal 90% confidence ranges ($\Delta\chi^2 = 2.706$).

^a Upper limit to the flux in the O K α blend (0.55–0.58 keV) assuming $N_H = 0.076 \times 10^{22}$ cm $^{-2}$

^b Flux in the 0.8–1.2 keV band assuming $N_H = 0.07 \times 10^{22}$ cm $^{-2}$, including unresolved contributions from Ne K α and other lines.

TABLE 2
LINE FLUX RATIOS IN THE SNR 0509–67.5

Line Ratio	<i>Chandra</i> ACIS-S	<i>XMM-Newton</i> EPIC-pn
O K α /Si K α	< 3.2	< 3.3
Fe L/Si K α	9.6	8.7
Si K β /Si K α	0.093 ± 0.018	0.069 ± 0.010
S K α /Si K α	0.27 ± 0.03	0.23 ± 0.02
Ar K α /Si K α	0.024 ± 0.009	0.032 ± 0.009
Ca K α /Si K α	0.0081 ± 0.0060	0.0098 ± 0.0044
Fe K α /Si K α	0.037 ± 0.017	0.030 ± 0.007

NOTE. — For simplicity, symmetric confidence ranges have been calculated taking the largest deviations from the fitted values in each case.

along § 5. First, we only model parameters that are consistent in both data sets. And second, the tolerance ranges that we use to compare models and data are much larger than the differences between ACIS-S and EPIC-pn that we have discussed here, and could easily accommodate the EPIC-MOS data sets as well.

5. SPECTRAL MODELING

5.1. Method, Parameters, and Strategy

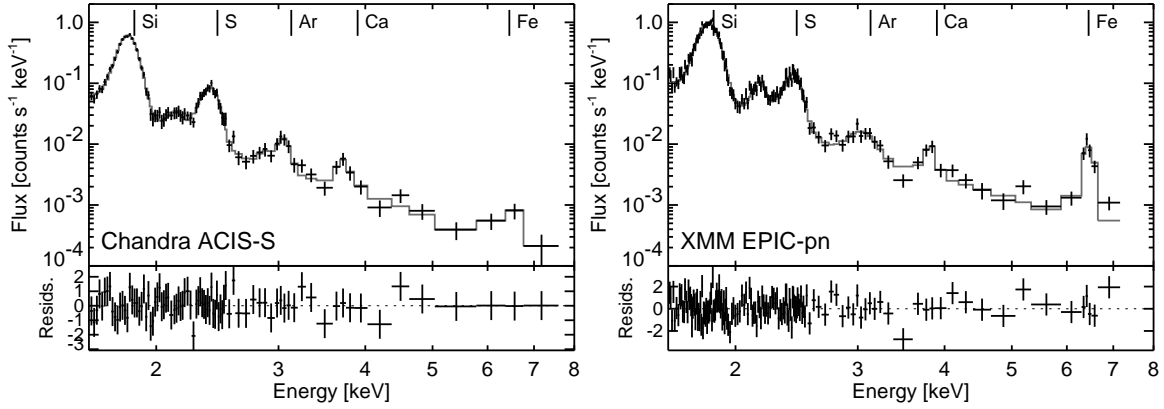


FIG. 4.— Spectral fits to the line emission in 0509–67.5 between 1.6 and 8.0 keV for *Chandra* ACIS-S (left) and *XMM-Newton* EPIC-pn (right). The expected centroids of the $K\alpha$ blends from the He-like ions of Si, S, Ar, and Ca, and the position of the Fe $K\alpha$ blend are indicated for reference.

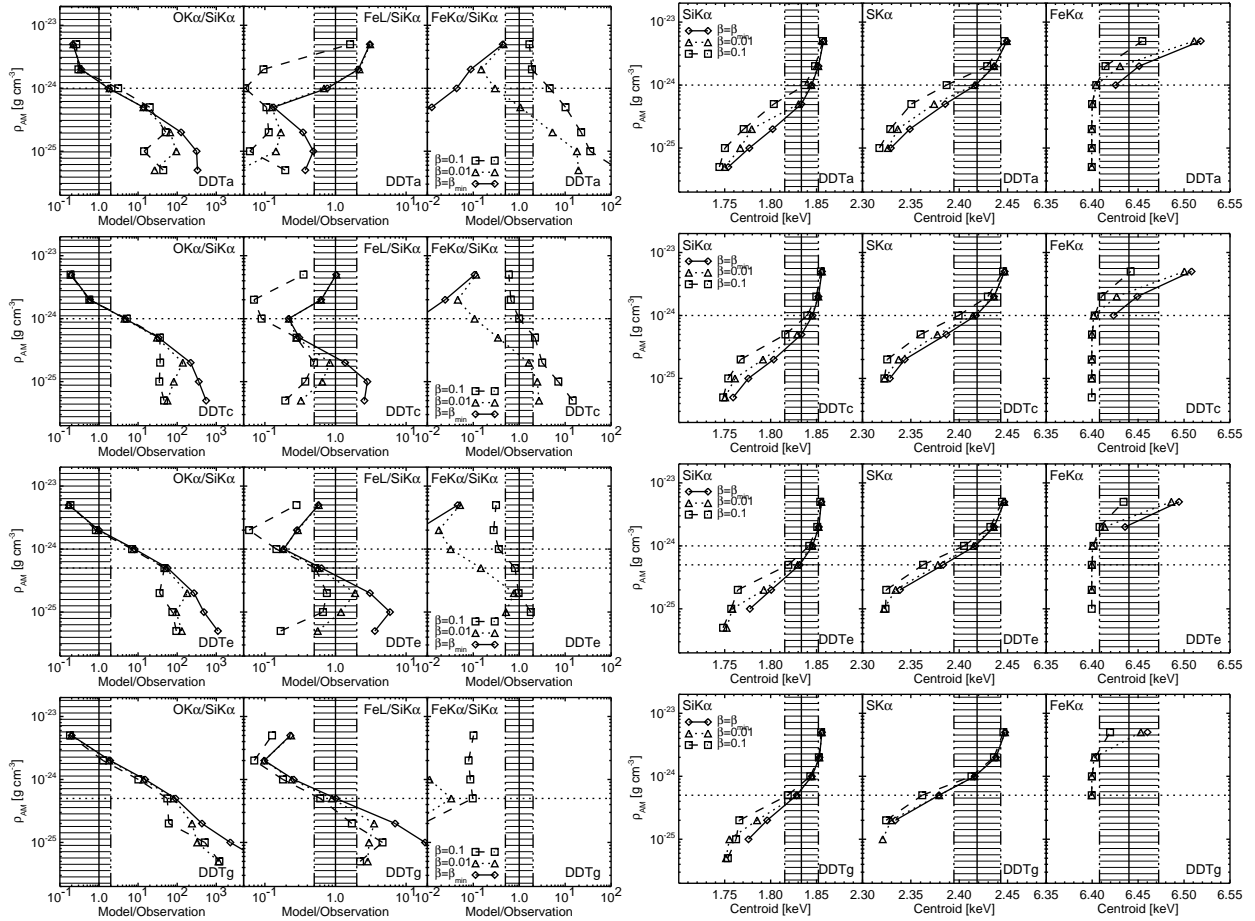


FIG. 5.— Fundamental line flux ratios (left panels) and line centroids (right panels) as a function of ρ_{AM} in the DDT models at $t = 400$ yr. For each model, the different values of β are plotted with solid lines and diamonds (β_{min}), dotted lines and triangles ($\beta = 0.01$), and dashed lines and squares ($\beta = 0.1$). The line flux ratios are normalized to the observed values (from Table 2), so that 1.0 is a perfect match. Tolerance ranges for line ratios and centroids are indicated by the striped regions around the observed values (vertical solid lines). The horizontal dotted lines mark the values of ρ_{AM} that satisfy the dynamic constraints at $t=400$ yr, as discussed in § 3.

To compare our grid of DDT models to the observations of SNR 0509–67.5, we have generated synthetic X-ray spectra for the shocked ejecta emission in our hydrodynamic simulations following the methods presented in Badenes et al. (2003, 2005a), with updated atomic data (Badenes et al. 2006), and including radiative and ionization losses with an isobaric approximation as described in Badenes et al. (2007). For a given Type Ia SN explosion model, the synthetic spectra are controlled by three variables only: AM density ρ_{AM} , SNR age t , and β . The parameter β represents the amount of collisionless electron heating at the reverse shock, and is defined as the ratio of specific internal energies in electrons and ions at the shock transition. It can take values between β_{min} , which represents mass proportional heating, and 1, which represents full equilibration (for more details, see § 2.2 in Badenes et al. 2005a). We have performed simulations in a grid of seven ρ_{AM} values (5×10^{-26} , 10^{-25} , 2×10^{-25} , 5×10^{-25} , 10^{-24} , 2×10^{-24} , and 5×10^{-24} g cm $^{-3}$) and three β values (β_{min} , 0.01, and 0.1). A similar, less extended grid of synthetic X-ray spectra based on DDT models was presented and discussed in Badenes et al. (2005b).

The ability of our synthetic spectra to reproduce SNR observations is limited by the quality of the atomic data in the spectral code. In the particular case of 0509–67.5, several important issues arise due to the low ionization state of the plasma. At ionization states below He-like, the atomic data for the K α blends of the major elements are reasonably complete, but deficiencies in K-shell transitions from higher levels should be expected in all elements. Atomic data in the Fe L complex are notably deficient, and altogether absent for ionization stages below Fe $^{+16}$ (Ne-like Fe). The strongest Fe L line in the *Chandra* HETG spectrum (at ~ 0.73 keV) can be associated with Ne-like Fe, and there are no signs of a significant contribution from lower ionization stages (Hughes et al., in preparation). Nevertheless, Fe L emission in the synthetic spectra should always be considered with caution as a matter of principle.

Given the limitations of the synthetic spectra listed above and the issues with the X-ray data described in § 4.2, we have chosen to focus our efforts on modeling only two fundamental quantities for which we can trust both models and observations. These include the centroids of the three brightest line blends (Si K α , S K α , and Fe K α), and the O K α /Si K α , Fe L/Si K α and Fe K α /Si K α line flux ratios, noting again that special care must be taken in the case of the Fe L/Si K α ratio. As we shall see, the combination of these parameters can constrain the kinetic energy of the SN explosion in the framework of the DDT models quite well. We will begin by using the DDT models at the nominal age of 400 yr in § 5.2, and then discuss variations of age in § 5.3 and alternative models in § 5.4. In § 5.5 we will go beyond our selection of diagnostic parameters to evaluate the performance of the models across the entire spectral range of *XMM-Newton*.

5.2. DDT Models at Nominal Age ($t=400$ yr)

A comparison between the observed line flux ratios and centroids and the predictions of the synthetic spectra generated by the DDT models in our grid at $t = 400$ yr is presented in Figure 5. In these plots, the observed

values (vertical solid lines) are the averages of the *Chandra* ACIS-S and *XMM-Newton* EPIC-pn values, except in the case of the Fe K α line, where only the *XMM-Newton* EPIC-pn data are taken into account. We note that the largest difference between ACIS-S and EPIC-pn in the relevant parameters corresponds to the the Fe L/Si K α ratio, and is only 9%. Tolerance ranges around the observed values are highlighted with striped regions: a factor 2 above and below for line flux ratios (except for the O K α /Si K α ratio, where only the upper limit is constrained), 1% for the Si K α and S K α centroids, and 0.5% for the Fe K α centroid. These tolerance ranges are rather large, mostly because of systematic uncertainties that are very hard to quantify (see § 5.2 in Badenes et al. 2006, for a discussion), and will only be used to provide some guidance in the comparisons between models and data. For each DDT model, the values of ρ_{AM} that satisfy the dynamical constraints from § 3 at $t = 400$ yr are indicated by horizontal dotted lines.

The combination of the O K α /Si K α and Fe K α /Si K α flux ratios clearly favors models with low O and high Fe emission. Only the DDT models with higher kinetic energies (and hence high Fe and low O yields), DDTa and DDTc, can reproduce both observables at the same time. When the dynamical constraints are brought into play, model DDTa (for $\rho_{AM} = 10^{-24}$ g cm $^{-3}$ and β between 0.01 and 0.1) performs better than model DDTc, because of its lower O K α flux. The Fe L/Si K α ratio also favors model DDTa over DDTc, although we stress that comparisons based on this parameter must be of a qualitative sort. The high Fe L/Si K α values found at low ρ_{AM} in models DDTc, DDTe and DDTg, for instance, are due mostly to Ne K emission, not to L-shell lines from shocked Fe. The line centroids plotted in the right hand panels of Figure 5 support the choice of model DDTa, but we note that the Fe K α centroid is slightly underpredicted at the ρ_{AM} imposed by the dynamical constraints.

The interplay between the constraints from the different line flux ratios with varying ρ_{AM} can be seen more clearly in Figure 6, where the sequence of DDT models has been mapped onto an E_k axis. The O K α /Si K α ratio can be reproduced by any model, provided that ρ_{AM} is high enough to ionize most O beyond the He-like stage at $t = 400$ yr. On the other hand, the Fe K α /Si K α ratio can only be reproduced by models with high E_k , where enough Fe has been shocked at $t = 400$ yr. These two flux ratios, together with the dynamical constraints clearly single out model DDTa with $\rho_{AM} = 10^{-24}$ g cm $^{-3}$. The Fe L/Si K α ratio confirms the choice, but we note again that the allowed region at low ρ_{AM} for this parameter is spurious. This plot highlights the remarkable agreement between the dynamical and X-ray spectral constraints on ρ_{AM} for the energetic DDT models, specially considering the large dynamic range of the diagnostic quantities shown in Figure 5. This is not a trivial coincidence, and it is not observed in other explosion models, as we shall see in 5.4. It indicates that the fundamental properties of the DDT models (exponential density profile, stratified ejecta) are well suited for SNR 0509–67.5.

5.3. DDT Models at Different Ages

The uncertainties in the age estimate from R05 (± 120 yr around the nominal age of 400 yr) stem from the un-

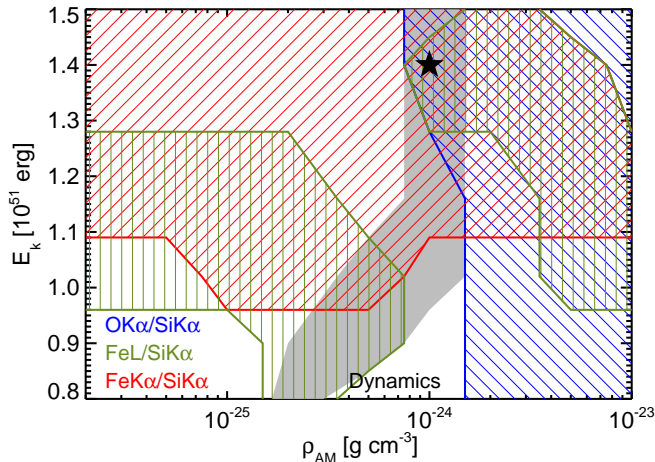


FIG. 6.— Global view of the performance of the DDT models (mapped onto an E_k axis) with varying ρ_{AM} at $t = 400$ yr. The striped regions represent the areas of the parameter space where the models can reproduce the observed O $K\alpha$ /Si $K\alpha$ (blue), Fe L/Si $K\alpha$ (green), and Fe $K\alpha$ /Si $K\alpha$ (red) line flux ratios for an optimum value of β . The dynamical constraints on ρ_{AM} are overlaid in gray. The star indicates the position of model DDTa at $\rho_{AM} = 10^{-24}$ g cm^{-3} , where all the constraints overlap.

known three-dimensional structure of the dust that is reflecting the light echo. The SNR dynamics are consistent with this range, but they impose a tight correlation between t and ρ_{AM} , as shown in § 3. Now we shall see that the properties of the X-ray emission from 0509–67.5 can substantially narrow down the age estimate, making large deviations from $t = 400$ yr seem unlikely. Higher ages require higher values of ρ_{AM} in order to reproduce the FS radius, and *vice versa* (see Figure 2). These changes in ρ_{AM} lead to major differences in the ionization timescale $\tau = \int n_e dt$ of the shocked ejecta, which rapidly drive several spectral parameters out of agreement with the observations. Two examples are presented in Figure 7, where the O $K\alpha$ /Si $K\alpha$ flux ratio and the centroid of the Si $K\alpha$ blend are compared with the observed values across the (ρ_{AM}, t) parameter space for model DDTa. At ages below 400 yr, most of the O is in the He-like ionization stage for the ρ_{AM} values imposed by the FS radius. This makes the O $K\alpha$ emission too strong, with O $K\alpha$ /Si $K\alpha$ ratios in excess of 5 times the observed value. Above 400 yr, the O $K\alpha$ /Si $K\alpha$ ratio is in the allowed region, but then the He-like ion of Si becomes dominant in the plasma, pushing the centroid toward higher energies that are incompatible with the value measured by *Chandra* and *XMM-Newton*. These comparisons are less favorable for the other DDT models, because their higher O content and lower E_k tend to increase the disagreement between the dynamical and spectral constraints.

One last constraint on the age of 0509–67.5 comes from the lack of recorded historical evidence for a recent SN in the LMC. A normal to bright Type Ia SN at a distance of 50 kpc would remain visible for several months, with an apparent visual magnitude around -1.0 at maximum light (the average extinction towards the LMC is 0.3 mag, Imara & Blitz 2007). Such an event would be hard to miss by even the most inattentive observers. European exploration of the southern hemisphere was well under way 400 years ago, led by skilled navigators who relied heavily on astronomy and monitored the night sky

whenever possible. Pieter Dirkszoon Keyser and Fredrik de Houtman mapped the southern sky (including Mensa and Doradus, which encompass the LMC) from Java between 1595 and 1597, noting the positions of all the stars brighter than 5th magnitude. In this island, the Dutch colony of Batavia (present day Jakarta, at 6°16' S latitude) and the English colony of Bantam became permanent around 1600. In South America, several Spanish settlements were thriving decades before that, including Lima (founded 1535, 12°12.6' S) and Buenos Aires (permanent since 1580, 34°36' S), from which the LMC is circumpolar. Even allowing for some incompleteness in the historical records, a spectacular astronomical event like a bright LMC supernova should have left some kind of trace if it happened at any time later than the beginning of the 17th century.

Taken together, the light echoes from the SN, the dynamic and spectral properties of the SNR, and the historical considerations, suggest an age very close to 400 yr for the birth event of 0509–67.5. The uncertainty around this value is hard to quantify, but deviations larger than a few decades seem unlikely, specially towards younger ages.

5.4. Other Models

We have seen that one-dimensional DDT models can reproduce the fundamental properties of the ejecta emission in 0509–67.5 with remarkable accuracy. It is outside the scope of this paper to perform an exhaustive exploration of other Type Ia explosion paradigms like Badenes et al. (2006) did for the Tycho SNR, but for the sake of completeness we discuss here some results obtained using other models. In Figure 8 we present the line flux ratios at $t = 400$ yr predicted by a sub-Chandrasekhar explosion (model SCH from Badenes et al. 2003) and a well-mixed 3D deflagration (model b30_3d_768 from Travaglio et al. 2004). In each case, we have overlaid the dynamical constraints on ρ_{AM} obtained with the procedure explained in § 3. The sub-Chandrasekhar model clearly shows that the overlap between spectral and dynamical constraints found in the energetic DDT models is not trivial, and indeed does not happen for the ejecta structure of this edge-lit WD detonation. The well-mixed 3D deflagration model has more severe problems: the presence of Fe and O everywhere in the ejecta leads to a systematic overprediction of the O $K\alpha$ /Si $K\alpha$ and Fe L/Si $K\alpha$ flux ratios at all values of ρ_{AM} .

5.5. Spatially Integrated Spectra

In the previous Sections we have taken the approach of focusing on a few parameters that can be both reliably extracted from the observations *and* confidently modeled with the existing spectral codes. This is a more meaningful and robust way of comparing synthetic spectra generated with HD+NEI models to data than the conventional method of χ^2 fitting across the entire X-ray band (for discussions, see Badenes et al. 2005a; Badenes et al. 2006). Nevertheless, it is always instructive to study the performance of the spectral models from a more global point of view. In Figure 9, we plot the synthetic spectra of the DDT models at $t = 400$ yr for the best value of ρ_{AM} within the dynamical constraints, together with the *XMM-Newton* EPIC-pn data

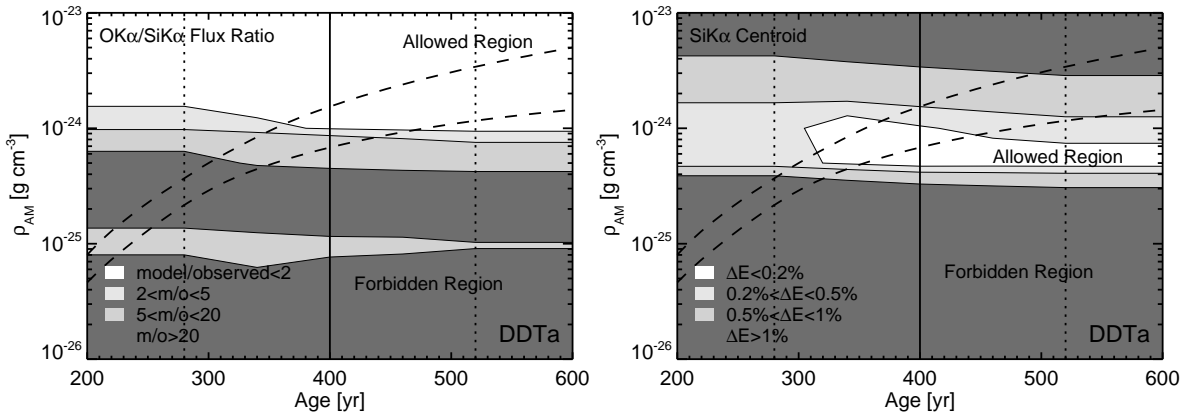


FIG. 7.— Comparison between the observations and the values predicted by the synthetic spectra produced from model DDTa for the O K α /Si K α flux ratio (left panel) and the centroid of the Si K α blend (right panel) as a function of ρ_{AM} and t . The black dashed plots are the dynamical constraints from the SNR radius from Figure 2. The age estimate from the light echoes is represented with the vertical solid and dotted lines.

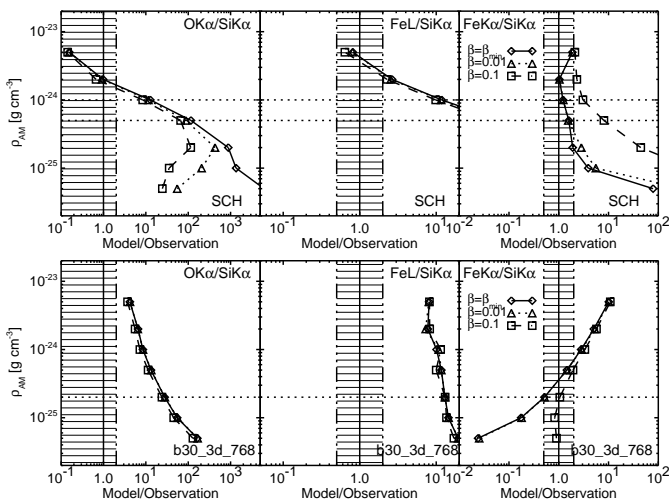


FIG. 8.— Fundamental line flux ratios as a function of ρ_{AM} from models SCH (top panels) and b30_3d_768 (bottom panels) at $t = 400$ yr. All labels and plots are as in Figure 5.

set. In each model, the value of β has been chosen to give the best approximation to the Fe K α /Si K α flux ratio: $\beta = 0.02$ for model DDTa and $\beta = 0.1$ for models DDTc, DDTe, and DDTg. No spectral fitting of any kind has been done. Instead, the ejecta models have been normalized to match the Si K α line and then a power law with the parameters determined in § 4.2 ($\alpha = 3.42$, $Norm = 3.5 \times 10^{-4}$ photons cm⁻² s⁻¹) has been added for the continuum. Absorption has been set to the fiducial $N_H = 0.07 \times 10^{22}$ cm² in all cases. By foregoing any spectral fitting, we can more easily compare the properties of the ejecta models to the data and to each other.

The performance of our model of choice, DDTa ($\rho_{AM} = 10^{-24}$ g cm⁻³, $\beta = 0.02$) is very good at all energies, albeit with some problems in localized areas. The flux in the Fe L complex is somewhat low, and the shape shows deviations from the observed spectrum. These discrepancies might be due mostly to the limitations in the atomic data discussed in § 5.1. Other problems are probably related to the explosion model, such as the deficit in the Mg K α flux and the low centroid of the Ca K α blend⁵. The degradation of the synthetic spectra along

the sequence of DDT models with decreasing E_k (or ρ_{tr}) is plain to see in Figure 9, specially in the behavior of the Fe and O emission. Normalization distances can be calculated for each model, yielding 36 kpc (DDTa), 51 kpc (DDTc), 23 kpc (DDTe), and 29 kpc (DDTg). Given the coarseness of our ρ_{AM} grid, values within $\sim 50\%$ of the distance to the LMC can be considered satisfactory. A more accurate study of the normalization distances cannot be justified without the inclusion of multidimensional effects in the HD+NEI simulations (see § 8.1 in Badenes et al. 2006).

We conclude this Section with a brief mention of the continuum emission. Detailed modeling of this component of the X-ray spectrum is outside the scope of the present work, but our HD+NEI calculations can help clarify the issue of its origin raised by WH04. At high energies (> 2 keV), the flux of the thermal AM emission in our HD+NEI models (for $\rho_{AM} = 10^{-24}$ g cm⁻³ and $t = 400$ yr at a distance of 50 kpc) is a factor 6 below the power law models listed in Table 1. This is a strong indication that the origin of the continuum emission in 0509–67.5 is indeed nonthermal.

6. DISCUSSION AND CONCLUSIONS

The light echo observations of R05 and R07 have turned 0509–67.5 into a unique object: the only X-ray bright SNR whose Type Ia origin is confirmed and whose explosion energy can be estimated based on spectroscopic information from its parent supernova. Motivated by these groundbreaking observations, we have re-examined the dynamics and X-ray spectrum of 0509–67.5, applying the HD+NEI modeling techniques introduced in Badenes et al. (2003) and Badenes et al. (2005a) to *Chandra* and *XMM-Newton* observations. We have based our analysis on a grid of one-dimensional DDT explosions, taking advantage of the relationship between ejecta structure and E_k in these models to place the birth event of 0509–67.5 in the sequence of dim to bright Type Ia SNe. Our conclusions are in excellent agreement with the light echo results of R07: SNR 0509–67.5 was originated by a bright, highly energetic Type Ia event of

($t = 430$ yr, $\rho_{AM} = 2 \times 10^{-24}$ g cm⁻³, $\beta = 0.03$) and the X-ray emission from the Tycho SNR. This suggests that the Mg content in our DDT models might be underestimated, and the distribution of Ca in the ejecta might be biased towards low densities.

⁵ The same two issues were noted by Badenes et al. (2006) in comparisons between the synthetic spectrum from model DDTc

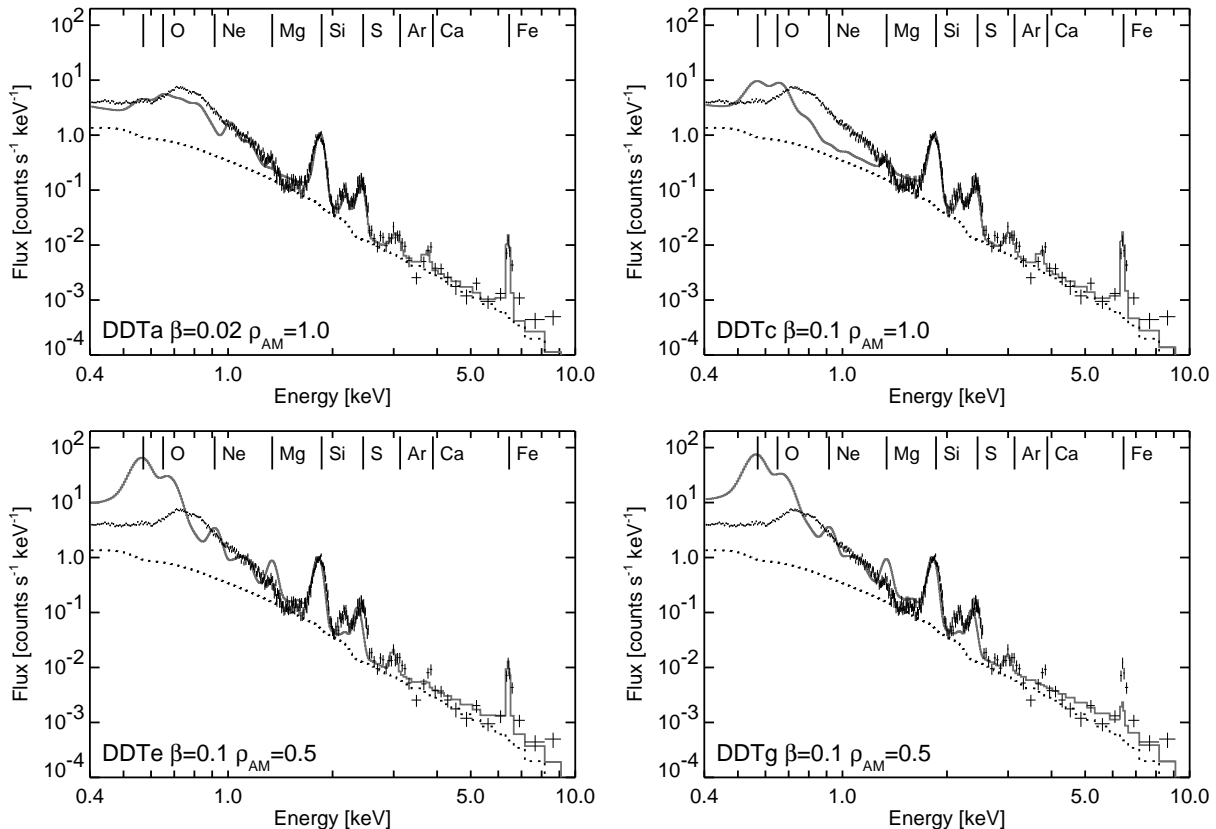


FIG. 9.— Comparison between the *XMM-Newton* EPIC-pn data set and the DDT model spectra at $t = 400$ yr for the most favorable values of β and ρ_{AM} (in units of 10^{-24} g cm $^{-3}$) within the dynamical constraints. Each ejecta model has been normalized to match the flux in the Si K α blend, and then a power law model with the parameters listed in Table 1 has been added. Absorption has been fixed at $N_H = 0.07 \times 10^{22}$ cm 2 . The position of the principal emission lines (K α and Ly α for O, K α for all other elements) has been indicated for clarity.

the subtype often referred to as SN 1991T-like. We thus present, for the first time, a scenario where the dynamics and X-ray spectrum of a Type Ia SNR form a consistent picture with the spectroscopy of its parent supernova.

Our preferred Type Ia explosion model, DDTa, has a kinetic energy of 1.40×10^{51} erg, and synthesizes $1.03 M_{\odot}$ of Fe, $0.09 M_{\odot}$ of Si, $0.07 M_{\odot}$ of S, $0.04 M_{\odot}$ of O, and $0.14 M_{\odot}$ of other elements (mostly Ar and Ca). The peak bolometric luminosity of this model is $\log L_{\text{bol}}(\text{ergs s}^{-1}) = 43.39$, and the amount of ^{56}Ni in the ejecta before nuclear decays is $0.97 M_{\odot}$. These values compare very well with the estimates for SN 1991T: $\log L_{\text{bol}} = 43.36$ (Contardo et al. 2000); $M_{^{56}\text{Ni}} = 0.87 M_{\odot}$ (Stritzinger et al. 2006, UVOIR method), $0.94 M_{\odot}$ (Stritzinger et al. 2006; Mazzali et al. 2007, B-band lightcurve method). The ejecta density and chemical composition profiles in model DDTa ($\rho_{AM} = 10^{-24}$ g cm $^{-3}$, $\beta = 0.02$) can reproduce very well both the dynamics (FS radius and velocity) and the fundamental properties of the X-ray spectrum (O, Si, S, and Fe emission) of 0509–67.5 at an age of 400 yr. Several dynamical, spectral, and historical arguments indicate that the SNR age cannot be very different from this value, which also coincides with the completely independent estimate derived by R05 from the geometry of the light echo.

These results, together with our previous work on the Tycho SNR (Badenes et al. 2006), constitute firm evidence that the phenomenological one-dimensional DDT models, which have proved so successful in explaining the

light curves and spectra of Type Ia SNe, are equally capable of reproducing the fundamental properties of the X-ray emission from young Type Ia SNRs. In particular, it is possible to use HD+NEI simulations based on these DDT models to estimate the kinetic energy (and ultimately the brightness) of a Type Ia SN explosion from the X-ray spectrum of its SNR. Hundreds of years after the SN explosion, the memory of the cataclysmic event persists in the X-rays from its SNR, opening a window onto ages past. This enables us to explore the relationship between individual dim/bright Type Ia SNe and their immediate surroundings (presence or absence of stellar formation, local metallicities, etc.) with much greater detail than is available to extragalactic studies (see Prieto et al. 2007). In the context of SNR research, having a good estimate for E_k can help to build better models for the impact of CR acceleration on the SNR dynamics. HD+NEI simulations have clearly become a powerful and flexible tool to study the relationship between SNRs and their parent SNe. For interested readers, the synthetic X-ray spectra from our models are available from the authors upon request.

We conclude with a reminder that much is left to do in the study of Type Ia SNe and their SNRs in general, and of 0509–67.5 in particular. Ongoing direct measurements of the ejecta and FS expansion using grating observations and proper motion studies should improve our knowledge of the dynamics of this SNR in the near future. Further work on the X-ray emission

should take the asymmetries of the object into account, in particular the enhanced Fe knots found by WH04. The one-dimensional models presented here can only sample the average or bulk properties of the shocked ejecta. Observational evidence for moderate asymmetries (Fesen et al. 2007; Gerardy et al. 2007) and clumping (Leonard et al. 2005; Wang et al. 2007) in the ejecta of Type Ia SNe is widespread, and SNR studies offer a unique opportunity to study these effects. This might provide crucial constraints for the multi-dimensional simulations of physically-motivated DDT explosions currently under way (Bravo & García-Senz 2006; Plewa 2007; Jordan et al. 2007)

The authors would like to thank Armin Rest, Tom Matheson, José L. Prieto, and the rest of the SuperMACHO team for their stimulating work on the light echoes from 0509–67.5 and for discussing several de-

tails of their results in advance of publication. CB also wishes to thank Edward van den Heuvel for his engaging presentation on the astronomical observations performed by Dutch explorers in the 17th century. Support for this work was provided by the National Aeronautics and Space Administration through Chandra Postdoctoral Fellowship Award Number PF6-70046 issued by the *Chandra* X-ray Observatory Center, which is operated by the Smithsonian Astrophysical Observatory for and on behalf of the National Aeronautics and Space Administration under contract NAS8-03060. Additional support was provided by the National Science Foundation under Grant No. PHY05-51164 to KITP-UCSB and by *Chandra* grant GO7-8068X to Rutgers University. E. B. has received support from the DURSI of the Generalitat de Catalunya and the Spanish DGICYT grants AYA 2004-06290-C02-02 and AYA 2005-08013-C03-01.

REFERENCES

- Alves, D. R. 2004, *New Astronomy Review*, 48, 659
- Badenes, C., Borkowski, K. J., & Bravo, E. 2005a, *ApJ*, 624, 198
- Badenes, C., Borkowski, K. J., Hughes, J. P., Hwang, U., & Bravo, E. 2006, *ApJ*, 645, 1373
- Badenes, C., Bravo, E., & Borkowski, K. J. 2005b, *Adv. Space Res.*, 35, 987
- Badenes, C., Bravo, E., Borkowski, K. J., & Domínguez, I. 2003, *ApJ*, 593, 358
- Badenes, C., Hughes, J. P., Bravo, E., & Langer, N. 2007, *ApJ*, 662, 472
- Baron, E., Bongard, S., Branch, D., & Hauschildt, P. H. 2006, *ApJ*, 645, 480
- Benetti, S., Cappellaro, E., Mazzali, P. A., Turatto, M., Altavilla, G., Bufano, F., Elias-Rosa, N., Kotak, R., Pignata, G., Salvo, M., & Stanishev, V. 2005, *ApJ*, 623, 1011
- Bravo, E. & García-Senz, D. 2006, *ApJ*, 642, L157
- Bravo, E., Tornambé, A., Domínguez, I., & Isern, J. 1996, *A&A*, 306, 811
- Cassam-Chenaï, G., Decourchelle, A., Ballet, J., Sauvageot, J.-L., Dubner, G., & Giacani, E. 2004, *A&A*, 427, 199
- Contardo, G., Leibundgut, B., & Vacca, W. D. 2000, *A&A*, 359, 876
- Ellison, D., Decourchelle, A., & Ballet, J. 2004, *A&A*, 413, 189
- Ellison, D. C., Patnaude, D. J., Slane, P., Blasi, P., & Gabici, S. 2007, *ApJ*, 661, 879
- Fesen, R. A., Höflich, P. A., Hamilton, A. J. S., Hammell, M. C., Gerardy, C. L., Khokhlov, A. M., & Wheeler, J. C. 2007, *ApJ*, 658, 396
- Gerardy, C. L., Meikle, W. P. S., Kotak, R., Höflich, P., Farrah, D., Filippenko, A. V., Foley, R. J., Lundqvist, P., Mattila, S., Pozzo, M., Sollerman, J., Van Dyk, S. D., & Wheeler, J. C. 2007, *ArXiv Astrophysics e-prints*
- Ghavamian, P., Blair, W. P., Sankrit, R., Hughes, J. P., & Raymond, J. C. 2007, *ArXiv Astrophysics e-prints*
- Höflich, P. & Khokhlov, A. 1996, *ApJ*, 457, 500
- Hughes, J. P., Hayashi, I., Helfand, D. J., Hwang, U., Itoh, M., Kirshner, R. P., Koyama, K., Markert, T., Tsunemi, H., & Woo, J. 1995, *ApJ*, 444, L81
- Imara, N. & Blitz, L. 2007, *ApJ*, 662, 969
- Iwamoto, K., Brachwitz, F., Nomoto, K., Kishimoto, N., Umeda, H., Hix, W., & Thielemann, F.-K. 1999, *ApJS*, 125, 439
- Jordan, G. I., Fisher, R., Townsley, D., Calder, A., Graziani, C., Asida, S., Lamb, D., & Truran, J. 2007, *ArXiv Astrophysics e-prints*
- Kasen, D. & Woosley, S. E. 2007, *ApJ*, 656, 661
- Khokhlov, A. M. 1991, *A&A*, 245, 114
- Leonard, D. C., Li, W., Filippenko, A. V., Foley, R. J., & Chornock, R. 2005, *ApJ*, 632, 450
- Marion, G. H., Höflich, P., Wheeler, J. C., Robinson, E. L., Gerardy, C. L., & Vacca, W. D. 2006, *ApJ*, 645, 1392
- Mazzali, P. A., Röpke, F. K., Benetti, S., & Hillebrandt, W. 2007, *Science*, 315, 825
- Phillips, M. 1993, *ApJ*, 413, L105
- Plewa, T. 2007, *ApJ*, 657, 942
- Prieto, J. L., Stanek, K. Z., & Beacom, J. F. 2007, *ArXiv e-prints*, 707
- Rakowski, C. E., Badenes, C., Gaensler, B. M., Gelfand, J. D., Hughes, J. P., & Slane, P. O. 2006, *ApJ*, 646, 982
- Rest, A., Matheson, T., Blondin, S., Bergmann, M., Welch, D. L., Suntzeff, N. B., Smith, R. C., Olsen, K., Prieto, J. L., Garg, A., Challis, P., Stubbs, C., Zenteno, A., Damke, G., Newman, A., Huber, M., Cook, K. H., Nikolaev, S., Becker, A. C., Miceli, A., Covarrubias, R., Morelli, L., Clocchiatti, A., & Minniti, D. 2007, *ApJ*, submitted [R07]
- Rest, A., Suntzeff, N. B., Olsen, K., Prieto, J. L., Smith, R. C., Welch, D. L., Becker, A., Bergmann, M., Clocchiatti, A., Cook, K., Garg, A., Huber, M., Miknaitis, G., Minniti, D., Nikolaev, S., & Stubbs, C. 2005, *Nature*, 438, 1132 [R05]
- Smith, R. K., Brickhouse, N. S., Liedahl, D. A., & Raymond, J. C. 2001, *ApJ*, 556, L91
- Stritzinger, M., Mazzali, P. A., Sollerman, J., & Benetti, S. 2006, *A&A*, 460, 793
- Travaglio, C., Hillebrandt, W., Reinecke, M., & Thielemann, F.-K. 2004, *A&A*, 425, 1029
- Wang, C.-Y. & Chevalier, R. 2001, *ApJ*, 549, 1119
- Wang, L., Baade, D., & Patat, F. 2007, *Science*, 315, 212
- Warren, J. & Hughes, J. 2004, *ApJ*, 608, 261 [WH04]
- Wheeler, J. C., Höflich, P., Harkness, R. P., & Spyromilio, J. 1998, *ApJ*, 496, 908
- Woosley, S. E., Kasen, D., Blinnikov, S., & Sorokina, E. 2007, *ApJ*, 662, 487



FIG. 10.— ‘The Persistence of Memory’, by Salvador Dalí, 1931. Oil on canvas, Museum of Modern Art, New York City. This painting by the genial Catalan artist represents the passage of time, and is very relevant to our work on SNR 0509–67.5 in a convoluted, surreal way. Dalí referred to the vaguely human figure in the center as the ‘paranoiac-critical Camembert’, for whatever that is worth.

APPENDIX

SOME REFLECTIONS ON THE RELEVANCE OF SURREALISM TO ASTROPHYSICS

The meaning of Salvador Dalí’s painting *The Persistence of Memory* (Figure 10) has been discussed at length elsewhere (see f.i. *MoMA Highlights*, New York: The Museum of Modern Art). The most common interpretation is that the famous ‘soft clocks’ are a metaphor for the passage of time, and the ants represent the inevitable consequence thereof: corruption of the flesh. Other interpretations are definitely possible, and equally valid - this being, after all, surrealism. Dalí once commented that the idea of the soft clocks came to him from the observation of a piece of Camembert cheese melting in the summer heat. Be that as it may, if the soft clocks *do* represent the passage of time, it is easy to draw an analogy between *The Persistence of Memory* and young SNRs like 0509–67.5. The X-ray observations of these objects open a window onto ages past, telling us what processes went on during the supernova explosions that originated them, and further back in time, how the supernova progenitor modified its surroundings. Just like a piece of melting Camembert cheese.